Study on Transport of Molecules in Gel by Surface-Enhanced Raman Spectroscopy

Samir Kumar (samiratwork@gmail.com)
 / Kyoto University https://orcid.org/0000-0002-6302-6326
Taneichi Taiga
Kyoto University: Kyoto Daigaku
Takao Fukuoka
Kyoto University: Kyoto Daigaku
Kyoko Namura
Kyoto University: Kyoto Daigaku
Motofumi Suzuki
Kyoto University: Kyoto Daigaku

Research Article

Keywords: Cellulose, SERS, Diffusion, Au nanorods

Posted Date: July 22nd, 2021

DOI: https://doi.org/10.21203/rs.3.rs-677741/v2

Study on Transport of Molecules in Gel by Surface-Enhanced Raman Spectroscopy

Samir Kumar, Taneichi Taiga, Takao Fukuoka, Kyoko Namura, Motofumi Suzuki**

Department of Micro Engineering, Graduate School of Engineering, Kyoto University, Katsura, Nishikyo, Kyoto, 615-8540, Japan

Corresponding Author

*SK: drsamirkumar2017@gmail.com, MS: m-snki@me.kyoto-u.ac.jp

ABSTRACT

Surface-enhanced Raman spectroscopy (SERS)-based biosensors have recently been extensively developed because of their high sensitivity and non-destructive nature. Conventional SERS substrates are unsuitable for detecting biomolecules directly from human skin. As a result, significant effort is being put into developing a gel-type SERS sensor that can segregate and detect biomolecules due to differences in molecular transport phenomena in the gel. However, no comprehensive research studies on the transport processes of molecules in gels in gel-type SERS sensors have been reported. This paper reports the differences in the transport phenomena of different molecules based on the time change of SERS spectrum intensity. The Au nanorod array substrate was coated with HEC gel to prepare a sample cell to study diffusion. The SERS spectra of aqueous solutions of 9 types of molecules were measured using the prepared sample cells. The rate at which each molecule diffuses into the gel differs depending on the molecule. The time variation of the characteristic SERS peak of each molecule was investigated based on a one-dimensional diffusion model, and the diffusion coefficient *D* was calculated for each molecule. A comparative study was conducted on the relationship between the diffusion coefficient and the molecular weight and molecular size, and it was found that the larger the molecular weight and molecular size, the slower the diffusion, which is based on the molecular motion theory and the inhibitory effect of the gel substance.

Keywords: Cellulose, SERS, Diffusion, Au nanorods

1. INTRODUCTION

Surface-enhanced Raman spectroscopy (SERS) is a vibrational spectroscopic technique that has emerged as a promising method for the non-destructive study of materials down to the single-molecule level.(Schlucker 2013)

SERS has proven to be a powerful analysis tool for molecular structure analysis, cell imaging, and biomolecule detection, among other things.(Kumar et al. 2015; El-Zahry and Lendl 2018; Yu et al. 2020; Hickey and He 2021) SERS has found its application not only in the fields of physics, chemistry, and biology, but also in engineering, pharmacy, and medicine.(McNay et al. 2011; Sharma et al. 2012; Bochenkov et al. 2015; Singh et al. 2019; Segawa et al. 2019a; Kumar et al. 2020c, d) Surface-enhanced Raman scattering is the phenomenon of enormous enhancement in the Raman scattering cross-section of molecules adsorbed in the vicinity of plasmonic nanoparticles.(Le Ru and Etchegoin 2009) Recently, SERS-based biosensors have been proposed for the detection of trace levels of biomolecules and diagnostics.(Kumar et al. 2015; Premasiri et al. 2018; Joseph et al. 2018) A SERS substrate is any nanostructure that supports SERS enhancement. Conventional SERS substrates are metal nanoparticles in either a colloidal solution or a solid substrate.(Suzuki et al. 2006; Rajput et al. 2017; Segawa et al. 2019b; Gahlaut et al. 2020; Yadav et al. 2021) As the colloidal solution is liquid and the structure of the solid substrate is rigid and brittle, it drastically limits the applicability of the SERS sensor and makes it unsuitable for detecting biomolecules directly from the human skin. As a result, a new gel-type porous SERS sensor that can collect biomarkers directly from the surface should be developed.

Yu and White have reported paper-based SERS devices for chromatographic separation and detection of target analytes in complex samples.(Yu and White 2013) Similarly, because of differences in the transport processes of biomolecules that permeate through the gel, gel-based SERS sensors may differentiate and detect biomolecules. If this technology is developed, it may serve as a biosensor and a new means of analyzing biomolecules. Recently, we reported a gel-based SERS sensor for the direct collection of biomarkers from the skin.(Kumar et al. 2019, 2020b) We found that the probe molecule solution permeated through the gel quickly and could be detected by SERS within 1 minute. However, no studies have been reported on the time-dependent SERS spectrum for the transport phenomena of various molecules and differences in transport phenomena in gels depending on the type of molecule. A few other reports on the gel-based SERS sensor and the diffusion studies of molecules in a gel.(Lauffer 1961; Muhr and Blanshard 1982; Amsden 1998; Samprovalaki et al. 2012; Tokita 2016; Sandrin et al. 2016; Chen et al. 2019a, b, 2021; Innocenzi and Malfatti 2019; Ogundare and van Zyl 2019; Wu et al. 2020; Kim et al. 2020; Hu et al. 2021) However, the focus of these studies was on the SERS enhancement and practical application of this sensor and theoretical studies on the diffusion of micro solutes in a homogeneous gel. To our knowledge, the transport phenomena of molecules with varying molecular weight in the gel have not been elucidated using SERS.

The diffusion of molecules is essential not only from a fundamental physics standpoint, but also for adequately evaluating the diffusion of drugs and particles,(Lock et al. 2018) transport of molecules in tumors,(Jain 1987) and release of small bioactive molecules from physical gels for the encapsulation and controlled release of small therapeutic molecules(Mayr et al. 2018). This study aims to elucidate the difference in transport phenomena of different types of molecules based on SERS spectral intensity time change. The time change of the SERS spectra of an aqueous solution of nine different molecules was studied using a Hydroxyethylcellulose (HEC) gel-based cell. A method for calculating the SERS spectral intensity from collected data and characterizing the transport of molecules in the gel was also developed. Finally, the temporal change in SERS spectral intensity was fitted using the model. The diffusion phenomena were quantified for nine types of molecules, and the relationship between molecular weight and molecular size and the diffusion phenomena was investigated.

2. MATERIALS AND METHOD

2.1 Gel and Raman probe molecules.

HEC gel, which is non-toxic to humans and is used as a thickening in cosmetics and external medicines, was used to prepare the gel-based cell for the experiment. HEC is a polymer compound in which a hydroxyl group is added to cellulose to make it water-soluble, and when mixed with water, it behaves as a transparent gel. The feasibility of a gel-based SERS sensor using HEC gel has been reported by Kumar et al.(Kumar et al. 2020b) HEC powder (SE400, Daicel FineChem Ltd.) was mixed with ultrapure water to a mass ratio of 10%, then well mixed and allowed to stand overnight or more to form an HEC gel from which bubbles were removed.

The molecular weight, molecular formula, van der Waals volume (vdW volume), and solvent-exposed surface area (SEA) of the nine types of Raman probes used in this study are shown in Table 1, and the molecular structure is shown in Figure S1 (Supplementary Information). The vdW volume of a molecule is defined as the space occupied by the molecule inaccessible to other molecules at room temperature(Askadskiĭ 2003), and SEA is defined as the surface area of a molecule in which the molecule can come into contact with the solvent.(Hamelryck 2005)

Table 1. Molecular weight, molecular formula, van der Waals volume, solvent exposure area of the molecule used for measurement.

Molecule name	Molecular weight	Molecular formula	vdW volume [Å^3]	Solvent exposure area [Å^2]
Pyridine	79.10	C_5H_5N	77.82	241.92
4,4'-Bipyridine	156.18	$C_{10}H_8N_8$	144.04	329.57
4,4'-Vinylenedipyridine	182.22	$C_{12}H_{10}N_2$	170.81	379.92
(S)-Equol	242.27	$C_{15}H_{14}O_3$	218.54	413.02
Acid Orange 7	350.32	$C_{16}H_{11}N_2NaO_4S$	263.99	548.08
Acid Orange 12	350.32	$C_{16}H_{11}N_2NaO_4S$	262.44	517.84
Crystal Violet	407.99	$C_{25}H_{30}ClN_3$	418.21	823.03
Rhodamine 6G	479.02	$C_{28}H_{31}ClN_2O_3$	377.39	765.18
Rose Bengal	1049.85	$C_{20}H_2Cl_4I_4K_2O_5$	420.68	610.65

2.2 Preparation of diffusion cells

The prepared sample cell is shown in Fig. **1**. A 1 mm thick silicone rubber was sliced into 20 mm × 25 mm pieces, with a 12 mm × 12 mm hole in the center. The prepared rubber was placed on a cover glass measuring 22 mm × 26 mm. A small amount of HEC gel was applied to the cover glass to prevent bubbles from forming between the SERS substrate and the cover glass, and then the SERS substrate was placed in the center and squeezed from above with tweezers. On the SERS substrate, HEC gel greater than the volume of the rubber hole was applied. The excessively applied HEC gel was horizontally scraped off from the surface of the rubber in the same manner as the doctor's blade technique to prepare an HEC gel layer with a constant film thickness.

On top of that, another piece of rubber was applied in an overlapping pattern. To account for the surface drying of the HEC gel over time, the sample cell was created immediately before each molecule measurement. The SERS spectrum was monitored after 100 μL of an aqueous solution of each Raman probe molecule was dropped from the top of the gel and covered with a cover glass.

2.3 Time-dependent SERS measurement and SERS chip

SERS spectra were acquired using a Raman spectrometer (RAM200S; LambdaVision Inc). A 785-nm laser with a 50× objective and approximately 30-mW power on the sample was used for excitation. 100-μL droplets of 1-mM aqueous solution of Raman probe molecules were deposited on the cell, and its SERS spectra were recorded as a function of time. Data was collected every 30 seconds for a total of 1800 seconds. After each acquisition, the sample

stage was shifted 50 μm to minimize the effect on the SERS spectrum caused by sample deterioration caused by repeated laser light irradiation of one place on the SERS substrate. Pyridine (PY), 4,4'-Bipyridine (BPY), 4,4'-Vinylenedipyridine (BPE), Crystal Violet (CV), Rhodamine 6G (Rh6G), and Rose Bengal (RB) have 1 s exposure duration and four accumulations. Since the SERS spectrum of (S)-Equol (SE), Acid Orange 7 (AO7), and Acid Orange 12 (AO12) is weaker than that of other molecules, the exposure time was kept at 5 s. OriginPro 2018 (OriginLab Corporation, Northampton, MA, USA) was used to process the SERS spectra and analyze the data. Before analysis, all data were baseline adjusted. A fourth-order polynomial was fitted to the raw SERS spectra and subtracted for baseline correction. For the diffusion analysis, the most intense peak area was selected.

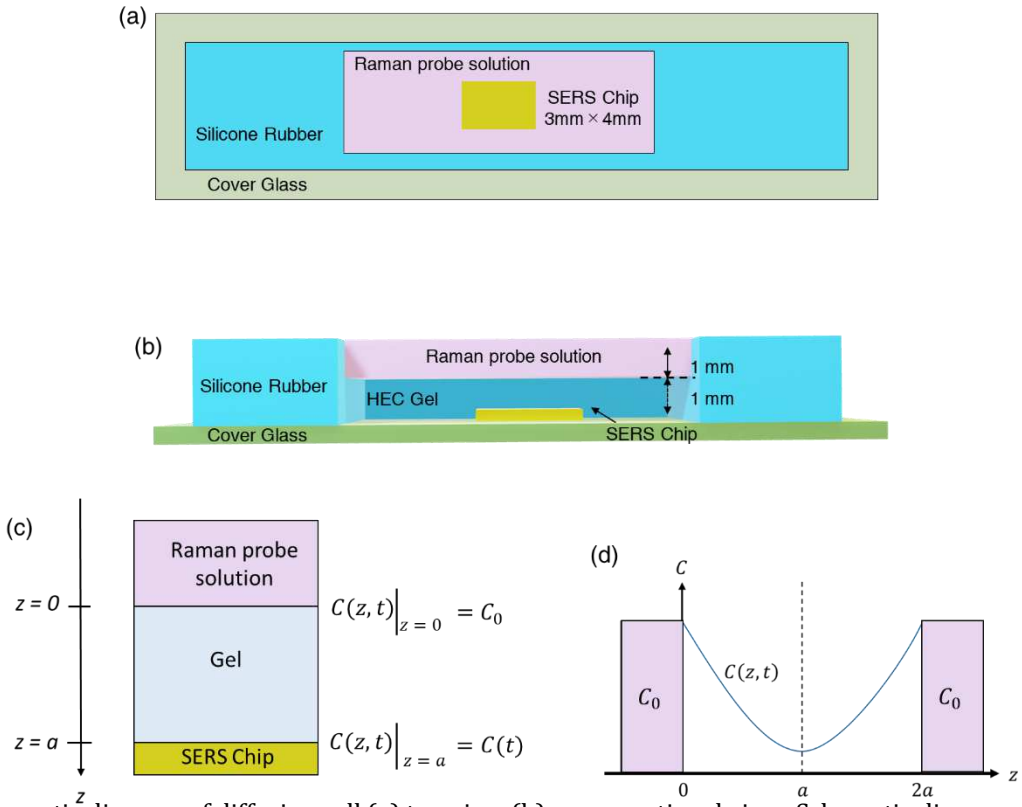

Fig. 1 Schematic diagram of diffusion cell (a) top view (b) cross-sectional view; Schematic diagram of cross-section of diffusion cell with boundary conditions; and (d) schematic diagram for the mirror image method to solve the diffusion equation.

The SERS chip was purchased from Nidek Co., Ltd, Japan. The SERS chip with elongated Au nanorod arrays (AuNRAs) was developed by Suzuki et al. and is now commercially available as the Wavelet (Supplementary information). The SERS chip was fabricated using a dynamic OAD technique.(Suzuki et al. 2005; Kumar et al. 2014, 2020a) The detailed fabrication process of AuNRAs can be found elsewhere.(Suzuki et al. 2007; Kumar et al. 2020e)

3. RESULTS AND DISCUSSION

3.1 Model for diffusion in gel

In this section, we will examine the method to evaluate the intensity of the measured SERS spectrum. We will evaluate a function that indicates the time change of the SERS spectral intensity. We will consider the diffusion of solutes in homogeneous solvents on a macro scale using the diffusion equation for simplicity. According to Fick's first law, a solute's diffusion flux is proportional to its concentration gradient. At this time, if the concentration is C (z, t) as a function of the coordinates z in the vertical direction and the time t, and the amount of solute transported through the unit area in the unit time is J, then

$$J = -D\frac{\partial C(z,t)}{\partial z} \quad (1)$$

Where D is the diffusion coefficient of the solute molecule. Simultaneously, the mass flowing into the region of height z and $z + \Delta z$ during time Δt is expressed as

$$J(z)\Delta t - J(z+\Delta z)\Delta t = -\frac{\partial J}{\partial z} \quad (2)$$

Since this is equal to the increase in solute concentration ΔC (z, t) during the time Δt, the following equation satisfies the continuity equation.

$$\frac{\partial C(z,t)}{\partial t} + \frac{\partial J}{\partial z} = 0 \quad (3)$$

The following equation is obtained from equations (1) and (2).

$$\frac{\partial C(z,t)}{\partial t} = D\frac{\partial^2 C(z,t)}{\partial z^2} \quad (4)$$

Equation 4 is called the diffusion equation. From kinetic theory, it is known that the diffusion coefficient is proportional to the inverse square root of the molecular weight. The higher the diffusion coefficient, the faster the diffusion. The transport processes of solutes can be described by providing the diffusion equation initial and boundary conditions, and the diffusion coefficient D can be used to quantify the diffusion of solutes. The diffusion equation of Eq. (4) is modeled in one dimension for the sample cell as shown in Fig. **1**(c), with the initial condition.

$$C(z,0)\Big|_{0<z\leq a} = 0 \quad (5)$$

and boundary condition

$$C(0,t) = C_0 = Const. \quad (6)$$

$$\left.\frac{\partial C(z,t)}{\partial z}\right|_{z=a} = 0 \quad (7)$$

As the molecules of interest are confined to a limited region and must satisfy the above boundary conditions in this region, the schematic diagram in Figure 1(c) was replaced with Figure 1(d) using the mirror image method. The solution of Eqn. 4 using the boundary conditions is given by

$$C(z,t) = C_0\left\{1 - \frac{4}{\pi}\sum_{n=0}^{\infty}\frac{1}{2n+1}\cdot\exp\left[-\left\{\frac{(2n+1)\pi}{2a}\right\}^2 Dt\right]\cdot\sin\left[\frac{(2n+1)\pi}{2a}z\right]\right\} \quad (8)$$

where a is the thickness of the gel layer. The detailed calculation can be found in the supplementary information.

By putting $z = a$ in the above equation, we get

$$C(a,t) = C(t) = C_0\left\{1 - \frac{4}{\pi}\sum_{n=0}^{\infty}\frac{(-1)^n}{2n+1}\cdot\exp\left[-\left\{\frac{(2n+1)\pi}{2a}\right\}^2 Dt\right]\right\} \quad (9)$$

Since the SERS spectral intensity of a molecule is proportional to its concentration,(Salemmilani et al. 2019; Wang et al. 2019) the SERS spectral intensity $S(t)$ can be written as

$$S(t) = S_0\left\{1 - \frac{4}{\pi}\sum_{n=0}^{\infty}\frac{(-1)^n}{2n+1}\cdot\exp\left[-\left\{\frac{(2n+1)\pi}{2a}\right\}^2 D'\right]\right\} \quad (10)$$

Equation 7 will be used for fitting the SERS intensity curve in the linear region. When the solute diffuses into the gel, it is considered to have three main diffusion inhibitory effects.(Lauffer 1961) The first is the interference of the gel with the diffusion of solutes due to the obstruction effect and increased hydrodynamic drag. The second is that the gel network may be thinner than the solute particles, and the third way the gel substance may affect the diffusion is by binding the solute.(Muhr and Blanshard 1982) These effects are accounted for in the diffusion coefficient D reported from the experiments in this study.

3.2 SERS measurement

First, let us consider the SERS spectrum of 4,4'-Bipyridine (BPY). BPY was chosen as the probe molecule because of its well-established vibrational bands and lack of fluorescence.(Joo 2004) Fig. **2**(a) shows the background and SERS spectrum after 1800 s when the Raman peak was well stabilized. The four prominent characteristic Raman bands of

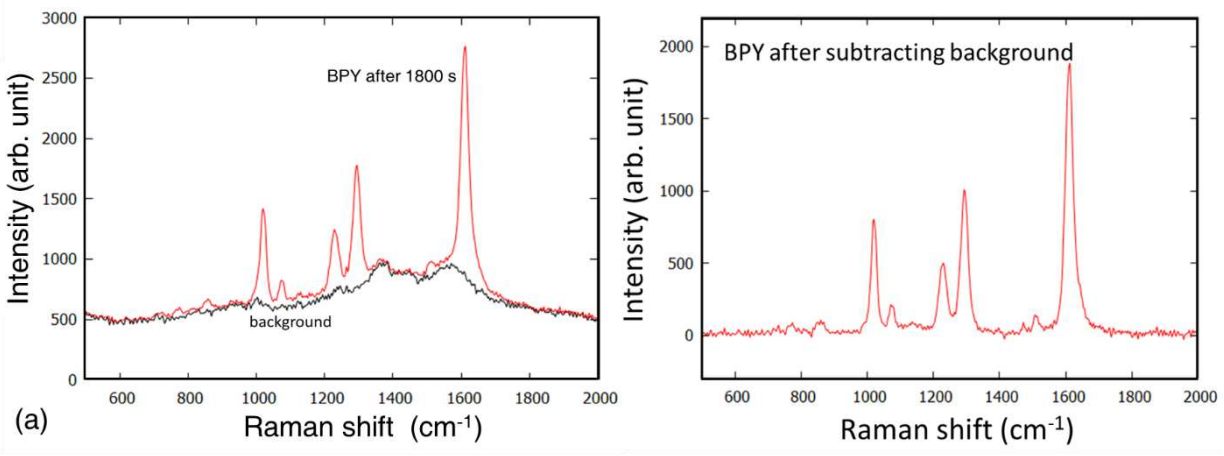

Fig. 2 (a) Background and SERS spectra of BPY and (b) difference spectra of BPY after 1800 s.

BPY at 1000, 1200, 1265, and 1600 cm^{-1} were observed, which are attributed to the pyridine ring breathing, ring deformation, C=C in-plane ring mode, and C=C stretching mode, respectively.(Lu et al. 1989) Fig. **2**(b) shows the difference spectrum obtained by subtracting the background spectrum from the SERS spectrum shown in Fig. **2**(a). Similar time-dependent difference spectra were also obtained for all the molecules by subtracting the background spectra from the SERS spectrum. Fig. **3** shows the difference spectra for BPY, CV, Rh6G, and RB. The same operation was performed for the other eight types of molecules. All the molecules diffused through the gel rapidly and reached the Au nanoparticles in less than 60s, giving SERS peaks. For all the molecules, the SERS peak was observed at the wavenumber unique to the molecule. In addition, Raman signal intensity increased continuously with time, indicating the process of an increase in the concentration of the molecular solute arriving at the AuNPs was driven by diffusion. BPE has the strongest peak intensity among the measured molecules, and SE, AO7, and AO12 exhibited the weakest peak intensity even after increasing the exposure period by five times. Furthermore, because Acid Orange 7 and Acid Orange 12 are structural isomers, their SERS spectra were identical.

3.3 Diffusion dependent SERS Intensity

Fig. **4** shows the highest peak area as a function of time. It is preferable to use the peak area because the peak widths of SERS and ordinary Raman are different.(Pérez-Jiménez et al. 2020) In the SERS spectrum of every molecule, the highest intensity peak was selected. The rise in the peak area can be considered directly proportional to the molecule concentration arriving at the AuNP *hotspot* and was used for estimating the coefficient of diffusion. This curve can be divided into three regions. In region I (red), probe molecules diffuse quickly within the gel and reach the AuNPs

giving the first SERS signal. The time interval corresponds to when the probe molecule covers a distance equal to the gel thickness. In region II (green), the peak intensity increases linearly and tends to saturate.

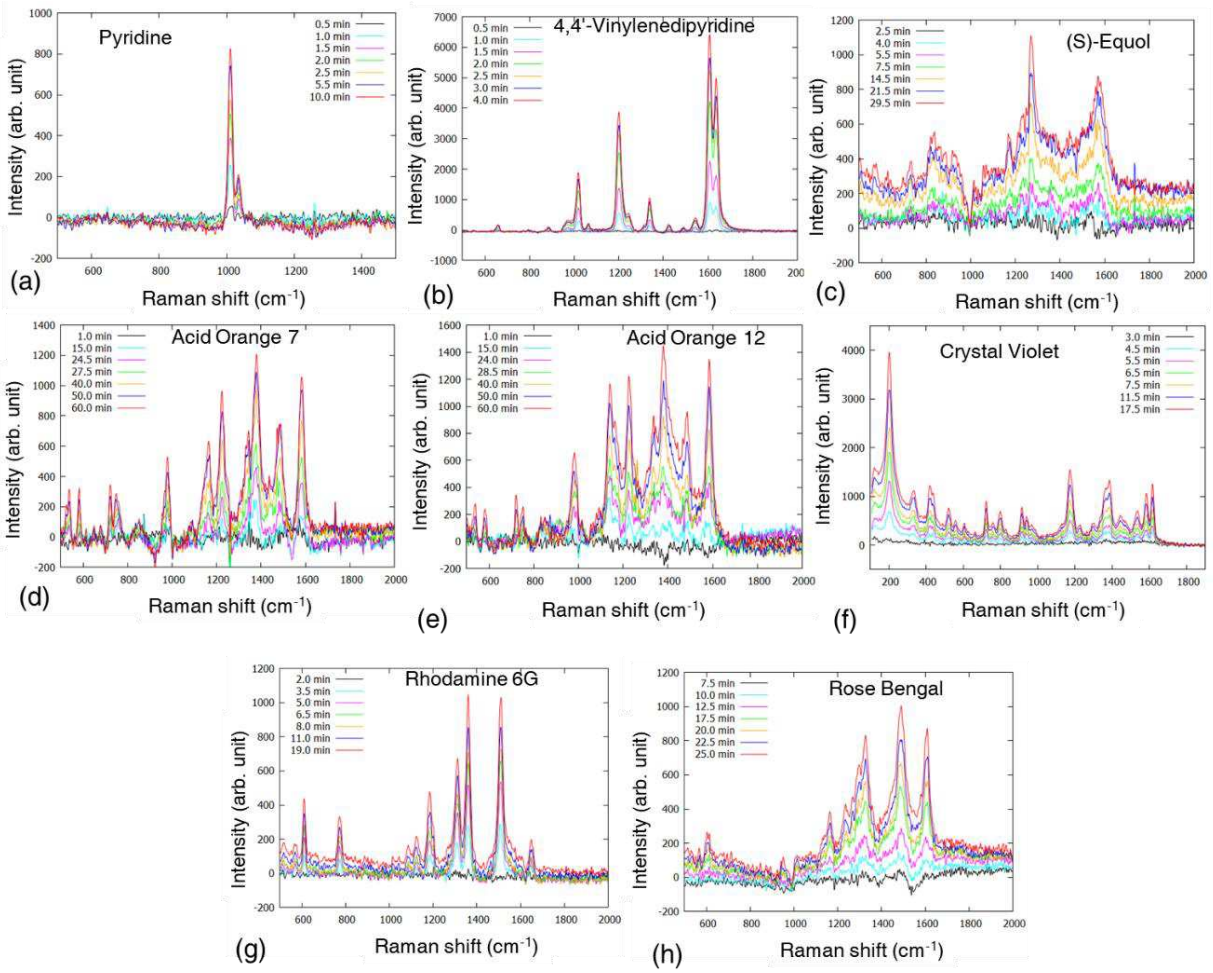

Fig. 3 Background subtracted SERS spectrum of (a) Pyridine, (b) 4,4-Vinylenedipyridine, (c) (S)-Equol, (d) Acid Orange 7, (e) Acid Orange 12, (f) Crystal Violet, (g) Rhodamine6G and (h) Rose Bengal, as a function of time.

The rise in peak intensity was found to be dependent upon the probe molecule. In other words, the transport phenomenon of molecules in the gel differs depending on the molecular weight. Additionally, region I and region II's width corresponds to the time of arrival and the time of saturation, respectively — was also found to depend on the probe molecule. In region III (blue), the SERS intensity attained a plateau and was almost constant. This implies that either the molecules have reached an equilibrium state with uniform concentration throughout the gel, or the number of available SERS hotspots has been occupied.

The diffusion coefficient can be calculated by slicing the gel after the experiment and measuring the concentration of solute as a function of time or by measuring the total amount of solute that penetrates the gel at a given time.(Lauffer

1961) To obtain the diffusion coefficient, we fitted the intensity-time curve using $S(t)$ examined as a model function previously for the gel film thickness of 0.8 mm. The linear portion of the curve was chosen for the fitting as it corresponds to the diffusion-limited transport regime where our boundary conditions are valid (Eq. [5] and Eq. [6]), see Figure 4.

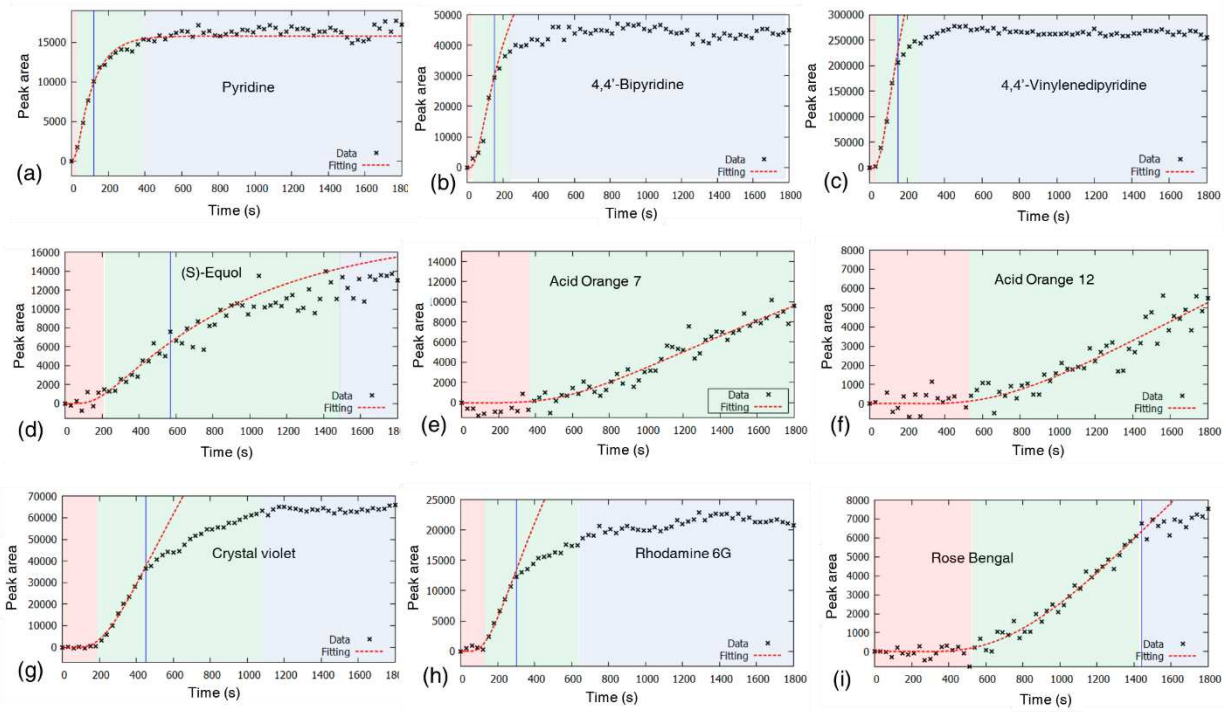

Fig. 4 Area of the highest peak as a function of time for (a) Pyridine, (b) 4,4-Bipyridine , (c) 4,4-Vinylenedipyridine, (d) (S)-Equol, (e) Acid Orange 7, (f) Acid Orange 12, (g) Crystal Violet, (h) Rhodamine6G , and (i) Rose Bengal. The dotted red curve is the fitted curve using Eq. 7, and the black cross points are the experimental data. The blue line is the boundary condition for the fitted curve. Regions I, II, and III are colored red, green, and blue, respectively.

The graph shows a strong agreement between the experimental data and the fit. Since Acid Orange 7 and Acid Orange 12 always showed a gradual increasing tendency across the measurement time (3 h), the fitting was done throughout the complete data set. **Table 2** shows the diffusion coefficient D of each molecule obtained by fitting.

Table 2. Diffusion coefficient D of the nine molecules

Molecule name	Diffusion coefficient D $[\,10^{-11}\mathrm{m}^2/\mathrm{s}\,]$
Pyridine	265
4,4'-Bipyridine	121
4,4'-Vinylenedipyridine	100
(S)-Equol	30.9
Acid Orange 7	8.72
Acid Orange 12	6.68
Crystal Violet	22.0
Rhodamine 6G	36.8
Rose Bengal	6.31

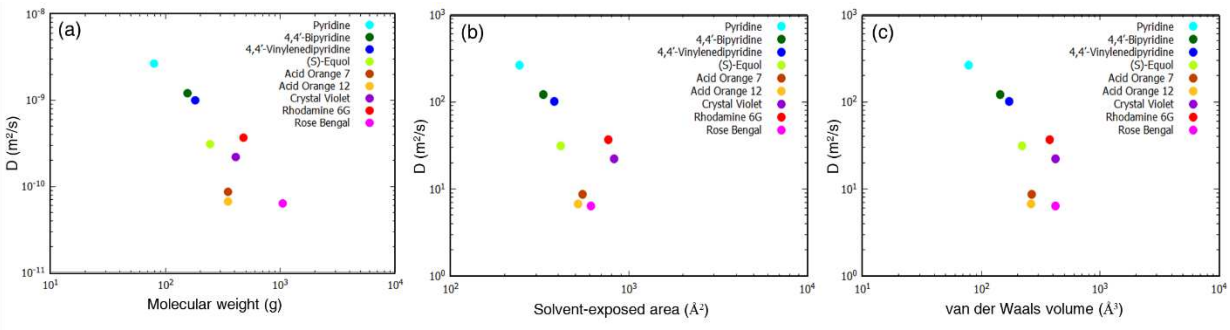

Fig. 5 Logarithmic plot of diffusion co-efficient as a function of (a) molecular weight, (b) solvent exposed area, (c) van der Waals volume.

We examined the diffusion coefficient as a function of molecular weight. Fig. **5**(a) shows the logarithmic plot of *D* as a function of molecular weight. In general, the diffusion coefficient was found to decrease with the increase in the molecular weight for all the probe molecules. Light molecules PY, BPY, and BPY were found to have the maximum, and the heavier molecules like RB were found to have the lower diffusion coefficient in the decreasing order of their molecular weight. This observation is consistent with the tendency based on the kinetic theory that molecules with smaller and lighter molecular weights diffuse faster in the solvent. However, when examined closely, Rh6G has a higher value of *D* than AO7, AO12, or CV; all three are lighter than Rh6G. Also, AO7 and AO12 have the value of D, which is almost like RB, which has almost thrice their molecular weight. Figures 5 (b) and 5 (c) show the diffusion coefficient plotted as a function of vdW volume and SEA to understand this strange behavior better. The diffusion coefficient D was found to have a similar tendency when plotted against vdW volume and SEA. This behavior is based on the inhibitory effect of the gel substance that tends to inhibit movement as the molecular size increases and the pathway length is extended. The trend was similar to the molecular weight for the lightest three molecules with the highest *D* value. Comparing CV and Rh6G, Rh6G has a higher molecular weight, while Crystal Violet has a higher vdW volume and SEA than Rh6G, explaining its lower D value. Therefore, it can be considered that the vdW volume and SEA are the major factors that affect the transport in the case of Rh6G. RB is the heaviest of all the test molecules and has the lowest diffusion *D* among the measured molecules.

Comparing the molecular size of RB with CV, the vdW volume is about the same, and the solvent exposure area is smaller than CV. However, CV has a higher *D*. As a result, when compared to CV, the molecular weight has a more significant effect on *D* in the case of RB. The two types of molecules, AO7 and AO12, have a small diffusion

coefficient *D,* even smaller than CV and Rh6G, even though they have smaller molecular weight values, vdW volume, and SEA. This is assumed to be because of chemical factors such as the activity of functional groups increasing due to the intricate molecular structure as the molecular weight and molecular size grow, affecting the molecule's diffusion. AO7 and AO12 have a hydroxyl group that may have an inhibitory effect on the gel and can delay the diffusion of molecules by binding the gel substance to the solvent. The three types of molecules with a large diffusion coefficient *D* do not have functional groups, and their molecular structures are relatively simple and like each other. Therefore, it is considered that a few chemical factors contribute to the difference in molecular transport phenomena.(Johansson et al. 1991, 2007) The difference in molecular diffusion was found to be based on the kinetic theory of molecules and the inhibitory effect of gel substances, which means that the larger the molecular weight and size of the molecule, the slower the diffusion.

4. CONCLUSIONS

In conclusion, we investigated the differences in transport processes of molecules of varying molecular weight as a function of SERS intensity when dispersed across HEC gel. We investigated a model function that can characterize this temporal change and derived the diffusion coefficient D for each molecule that matches the experimental observations. The diffusion coefficient D was examined in connection with the molecular weight, vdW volume, and solvent exposure area. This investigation agrees with prior observations based on the molecular motion concept that diffusion slows as molecular weight and size increase and the inhibitory effect of the gel substance.

Supplematary Information

The molecular structure of probe molecules, the diffusion model in detail, and the SEM images of the SERS chip utilized for this study can be found in the supplementary information.

Acknowledgments

Funding. This work was supported by JST COI under Grant Number JPMJCE1307.

Declarations

Conflict of interest. The authors have no conflicts of interest to declare.

Human and animal rights. This article does not contain any studies with human participants or animals performed by any of the authors.

REFERENCES

Amsden B (1998) Solute Diffusion within Hydrogels. Mechanisms and Models. Macromolecules 31:8382–8395

Askadskiĭ AA (2003) Computational materials science of polymers. Cambridge Int Science Publishing

Bochenkov V, Baumberg J, Noginov M, et al (2015) Applications of plasmonics: general discussion. Faraday Discuss 178:435–466

Chen J, Huang M, Kong L, Lin M (2019a) Jellylike flexible nanocellulose SERS substrate for rapid in-situ non-invasive pesticide detection in fruits/vegetables. Carbohydr Polym 205:596–600

Chen Y-C, Chen J-J, Hsiao Y-J, et al (2021) Plasmonic gel films for time-lapse LSPR detection of hydrogen peroxide secreted from living cells. Sens Actuators B Chem 336:129725

Chen Y-C, Chen K-Y, Hsu K-H, Chen Y-F (2019b) Surface-enhanced Raman spectroscopy and localized surface plasmon resonance detection of hydrogen peroxide using plasmonic gels. In: Plasmonics in Biology and Medicine XVI. International Society for Optics and Photonics, p 108940R

El-Zahry MR, Lendl B (2018) Structure elucidation and degradation kinetic study of Ofloxacin using surface enhanced Raman spectroscopy. Spectrochim Acta A Mol Biomol Spectrosc 193:63–70

Gahlaut SK, Savargaonkar D, Sharan C, et al (2020) SERS platform for dengue diagnosis from clinical samples employing a hand held Raman spectrometer. Anal Chem 92:2527–2534

Hamelryck T (2005) An amino acid has two sides: a new 2D measure provides a different view of solvent exposure. Proteins 59:38–48

Hickey ME, He L (2021) SERS imaging analyses of bacteria cells among plant tissues. Talanta 225:122008

Hu X, Yang B, Wen X, et al (2021) One-pot synthesis of a three-dimensional Au-decorated cellulose nanocomposite as a surface-enhanced Raman scattering sensor for selective detection and in situ monitoring. ACS Sustain Chem Eng. https://doi.org/10.1021/acssuschemeng.0c09296

Innocenzi P, Malfatti L (2019) Mesoporous materials as platforms for surface-enhanced Raman scattering. Trends Analyt Chem 114:233–241

Jain RK (1987) Transport of molecules in the tumor interstitium: a review. Cancer Res 47:3039–3051

Johansson L, Elvingson C, Skantze U, Löfroth JE (2007) Diffusion and interaction in gels and solutions. In: Progress in Colloid & Polymer Science. Steinkopff, Darmstadt, pp 25–29

Johansson L, Skantze U, Loefroth JE (1991) Diffusion and interaction in gels and solutions. 2. Experimental results on the obstruction effect. Macromolecules 24:6019–6023

Joo S-W (2004) Surface-enhanced Raman scattering of 4,4′-bipyridine on gold nanoparticle surfaces. Vib Spectrosc 34:269–272

Joseph MM, Narayanan N, Nair JB, et al (2018) Exploring the margins of SERS in practical domain: An emerging diagnostic modality for modern biomedical applications. Biomaterials 181:140–181

269 Kim DJ, Yoon J, Kim D-H, et al (2020) Plasmonic microgels for Raman-based molecular detection created by
270 simultaneous photoreduction and photocross-linking. ACS Appl Mater Interfaces 12:48188–48197

271 Kumar S, Doi Y, Namura K, Suzuki M (2020a) Plasmonic nanoslit arrays fabricated by serial bideposition: Optical
272 and surface-enhanced Raman scattering study. ACS Applied Bio Materials

273 Kumar S, Goel P, Singh DP (2014) Fabrication of superhydrophobic silver nanorods array substrate using glancing
274 angle deposition. AIP Conf Proc

275 Kumar S, Kanagawa M, Namura K, et al (2020b) Multilayer thin-film flake dispersion gel for surface-enhanced
276 Raman spectroscopy. Appl Nanosci. https://doi.org/10.1007/s13204-020-01562-0

277 Kumar S, Kumar P, Das A, Shakher Pathak C (2020c) Surface-Enhanced Raman Scattering: Introduction and
278 Applications. In: Recent Advances in Nanophotonics - Fundamentals and Applications. IntechOpen

279 Kumar S, Lodhi DK, Goel P, et al (2015) A facile method for fabrication of buckled PDMS silver nanorod arrays as
280 active 3D SERS cages for bacterial sensing. Chem Commun 51:12411–12414

281 Kumar S, Namura K, Kumaki D, et al (2020d) Highly reproducible, large scale inkjet-printed Ag nanoparticles-ink
282 SERS substrate. Results in Materials 8:100139

283 Kumar S, Namura K, Suzuki M (2019) Proposal for a gel-based SERS sensor. In: Plasmonics in Biology and Medicine
284 XVI. International Society for Optics and Photonics, p 1089414

285 Kumar S, Tokunaga K, Namura K, et al (2020e) Experimental evidence of a twofold electromagnetic enhancement
286 mechanism of surface-enhanced Raman scattering. J Phys Chem C Nanomater Interfaces 124:21215–21222

287 Lauffer MA (1961) Theory of diffusion in gels. Biophys J 1:205–213

288 Le Ru EC, Etchegoin PG (2009) SERS enhancement factors and related topics. In: Principles of Surface-Enhanced
289 Raman Spectroscopy. Elsevier, pp 185–264

290 Lock JY, Carlson TL, Carrier RL (2018) Mucus models to evaluate the diffusion of drugs and particles. Adv Drug
291 Deliv Rev 124:34–49

292 Lu T, Cotton TM, Birke RL, Lombardi JR (1989) Raman and surface-enhanced Raman spectroscopy of the three
293 redox forms of 4,4'-bipyridine. Langmuir 5:406–414

294 Mayr J, Saldías C, Díaz Díaz D (2018) Release of small bioactive molecules from physical gels. Chem Soc Rev
295 47:1484–1515

296 McNay G, Eustace D, Smith WE, et al (2011) Surface-enhanced Raman scattering (SERS) and surface-enhanced
297 resonance Raman scattering (SERRS): a review of applications. Appl Spectrosc 65:825–837

298 Muhr AH, Blanshard JMV (1982) Diffusion in gels. Polymer 23:1012–1026

299 Ogundare SA, van Zyl WE (2019) A review of cellulose-based substrates for SERS: fundamentals, design principles,
300 applications. Cellulose 26:6489–6528

301 Pérez-Jiménez AI, Lyu D, Lu Z, et al (2020) Surface-enhanced Raman spectroscopy: benefits, trade-offs and future
302 developments. Chem Sci 11:4563–4577

303 Premasiri WR, Chen Y, Fore J, et al (2018) SERS Biomedical Applications: Diagnostics, Forensics, and Metabolomics.
304 In: Frontiers and Advances in Molecular Spectroscopy. Elsevier, pp 327–367

Rajput A, Kumar S, Singh JP (2017) Vertically standing nanoporous Al–Ag zig-zag silver nanorod arrays for highly active SERS substrates. Analyst 142:3959–3966

Salemmilani R, Mirsafavi RY, Fountain AW, et al (2019) Quantitative surface-enhanced Raman spectroscopy chemical analysis using citrate as an in situ calibrant. Analyst 144:1818–1824

Samprovalaki K, Robbins PT, Fryer PJ (2012) Investigation of the diffusion of dyes in agar gels. J Food Eng 111:537–545

Sandrin D, Wagner D, Sitta CE, et al (2016) Diffusion of macromolecules in a polymer hydrogel: from microscopic to macroscopic scales. Phys Chem Chem Phys 18:12860–12876

Schlucker S (ed) (2013) Surface enhanced Raman spectroscopy, 1st edn. Wiley-VCH Verlag, Weinheim, Germany

Segawa H, Fukuoka T, Itoh T, et al (2019a) Rapid detection of synthetic cannabinoids in herbal highs using surface-enhanced Raman scattering produced by gold nanoparticle co-aggregation in a wet system. Analyst 144:6928–6935

Segawa H, Fukuoka T, Itoh T, et al (2019b) Rapid detection of hypnotics using surface-enhanced Raman scattering based on gold nanoparticle co-aggregation in a wet system. Analyst 144:2158–2165

Sharma B, Frontiera RR, Henry A-I, et al (2012) SERS: Materials, applications, and the future. Mater Today (Kidlington) 15:16–25

Singh N, Kumar P, Riaz U (2019) Applications of near infrared and surface enhanced Raman scattering techniques in tumor imaging: A short review. Spectrochim Acta A Mol Biomol Spectrosc 222:117279

Suzuki M, Maekita W, Kishimoto K, et al (2005) Direct formation of arrays of prolate Ag nanoparticles by dynamic oblique deposition. Jpn J Appl Phys (2008) 44:L193–L195

Suzuki M, Maekita W, Wada Y, et al (2006) In-line aligned and bottom-up Ag nanorods for surface-enhanced Raman spectroscopy. Appl Phys Lett 88:203121

Suzuki M, Nakajima K, Kimura K, et al (2007) Au nanorod arrays tailored for surface-enhanced Raman spectroscopy. Anal Sci 23:829–833

Tokita M (2016) Transport Phenomena in Gel. Gels 2:. https://doi.org/10.3390/gels2020017

Wang YY, Jiang J, Yin J, et al (2019) Determination of concentration of adsorbed molecules by Raman spectroscopy and optical imaging. J Appl Phys 125:244305

Wu L-A, Chen Y-C, Pai W-C, et al (2020) Plasmonic nanoparticles in agarose gel and filter paper-integrated microfluidic devices for SERS detection of molecules. In: Plasmonics in Biology and Medicine XVII. International Society for Optics and Photonics, p 1125702

Yadav S, Senapati S, Desai D, et al (2021) Portable and sensitive Ag nanorods based SERS platform for rapid HIV-1 detection and tropism determination. Colloids Surf B Biointerfaces 198:111477

Yu WW, White IM (2013) Chromatographic separation and detection of target analytes from complex samples using inkjet printed SERS substrates. Analyst 138:3679–3686

Yu X, Li W, Liang O, et al (2020) Molecular orientation and specificity in the identification of biomolecules via surface enhanced Raman spectroscopy. Anal Biochem 599:113709

342

343

344

Supplementary Files

This is a list of supplementary files associated with this preprint. Click to download.

- SERSDiffusionESI20210602v1.pdf